J Exp Biol Advance Online Articles. First posted online on 1 June 2015 as doi:10.1242/jeb.118059
Access the most recent version at http://jeb.biologists.org/lookup/doi/10.1242/jeb.118059

Minor Contributions of the Maxillary Sinus to the Air-conditioning Performance in Macaque Monkeys

Futoshi Mori[1,2,**], Sho Hanida[3], Kiyoshi Kumahata[4], Takako Miyabe-Nishiwaki[5], Juri Suzuki[5], Teruo Matsuzawa[6], and Takeshi D. Nishimura[5,*]

[1] Interfaculty Initiative in Information Studies, The University of Tokyo, Bunkyo-ku, Tokyo 113-0032, Japan

[2] Earthquake Research Institute, The University of Tokyo, Bunkyo-ku, Tokyo 113-0032, Japan

[3] Kanazawa Institute of Technology, Nonoichi, Ishikawa 921-8501, Japan

[4] RIKEN Advanced Institute for Computational Science, Kobe, Hyogo 650-0047, Japan

[5] Primate Research Institute, Kyoto University, Inuyama, Aichi 484-8506, Japan

[6] Japan Advanced Institute of Science and Technology, Nomi, Ishikawa 923-1292, Japan

[*]Corresponding author: Takeshi Nishimura, D.Sc.
Primate Research Institute, Kyoto University
41-2 Kanrin, Inuyama, Aichi 484-8506, Japan
telephone +81-568-63-0534
e-mail nishimura.takeshi.2r@kyoto-u.ac.jp

**Current address:
Institute for Biomedical Science, Iwate Medical University, Yahaba, Iwate 028-3694, Japan

ABSTRACT

The nasal passages mainly adjust the temperature and humidity of inhaled air to reach the alveolar condition required in the lungs. By contrast to most other nonhuman primates, macaque monkeys are distributed widely among tropical, temperate and subarctic regions, and thus some species need to condition the inhaled air in cool and dry ambient atmospheric areas. The internal nasal anatomy is believed to have undergone adaptive modifications to improve the air-conditioning performance. Furthermore, the maxillary sinus (MS), an accessory hollow communicating with the nasal cavity, is found in macaques, whereas it is absent in most other extant Old World monkeys, including savanna monkeys. In this study, we used computational fluid dynamics simulations to simulate the airflow and heat and water exchanges over the mucosal surface in the nasal passage. Using the topology models of the nasal cavity with and without the MS, we demonstrated that the MS makes little contribution to the airflow pattern and the air-conditioning performance within the nasal cavity in macaques. Instead, the inhaled air is conditioned well in the anterior portion of the nasal cavity before reaching the MS in both macaques and savanna monkeys. These findings suggest that the evolutionary modifications and coetaneous variations in the nasal anatomy are rather independent of transitions and variations in the climate and atmospheric environment found in the habitats of macaques.

INTRODUCTION

Macaque monkeys, genus *Macaca*, are a group of Old World monkeys (OWMs) in the family Cercopithecidae (Fooden, 1980; Fleagle, 2013). At present, macaques are distributed widely in western to eastern Asia and in a restricted region of North Africa (Fooden, 1980; Smith et al., 2005). They show the second-largest geographic distribution after humans among primates. This group probably arose in northern Africa in the Late Miocene, before expanding their distribution into Eurasia during the latest Miocene and then dispersing to East Asia by the Late Pliocene (Delson, 1980; Alba et al., 2014). Their adaptive radiation resulted in their successful colonization of more varied climates and ecological environments compared with other OWMs (Fleagle, 2013). In particular, the Japanese macaque, *Macaca fuscata*, expanded its distribution throughout the Japanese Archipelago from subtropical into subarctic zones, which are the highest latitudes inhabited by non-human primates (Fooden, 1980). These ecogeographic features are reflected partly by the broad morphological variations in terms of the body size and the shapes of surface features within this genus (Fooden and Albrecht, 1993; Pan and Oxnard, 2000; Ito et al., 2014).

The nasal cavity allows the inhaled air to flow from the external nostril into the pharyngeal region (Cole, 1982; Elad et al., 2008). The nasal cavity conditions the respiratory air, as well as performing other functions such as olfactory sensing, dust filtering and voice resonance (Cole, 1982; Elad et al., 2008). The nasal cavity behind the nasal vestibule is divided into the three thin channels, which are referred to as the inferior, middle and superior meatuses with the olfactory cleft. The three meatuses are separated by two major thin bony plates that are covered by respiratory mucosa, which are referred to as the conchae or turbinates (Cave, 1973; Cole, 1982; Harkema et al., 1987; Elad et al., 2008). The inhaled air flows over the mucosal surface, exchanges heat and water with the mucosal tissues and is adjusted to the alveolar condition—i.e., fully saturated at body temperature—before it reaches the lung. This means that increasing the surface area of the respiratory mucosa improves the air-conditioning performance. Indeed, the bony nasal cavity is widened and enlarged in the population of Japanese macaques that inhabit the northern (colder and dryer) region compared with those in southern (warmer and wetter) regions (Rae et al., 2003). Inadequate air conditioning

damages the mucosal tissues of the respiratory system and also impairs the respiratory performance, thereby endangering the health and affecting the survival of animals. The nasal cavity anatomy is often regarded as being evolutionarily sensitive to the ambient atmospheric conditions of a habitat in macaques (Rae et al., 2003; Marquez and Laitman, 2008) Thus, the current ecogeographic range of macaques may depend partly on evolutionary modifications in their nasal anatomy to improve the air-conditioning performance.

The maxillary sinus (MS) is one of the paranasal sinuses, which communicates with the middle meatus of the nasal cavity via a narrow opening called the ostium and pneumatizes the maxilla (Rae and Koppe, 2004; Rossie, 2008). This bony sinus is lined with respiratory mucosa that extends from the nasal cavity through the ostium (Rae and Koppe, 2004; Rossie, 2008). MS pneumatization is always found in macaques and sometimes in baboons and gelada (*Papio* and *Theropithecus*), whereas it is absent in other extant OWMs (Koppe and Ohkawa, 1999; Nishimura et al., 2014). This feature is believed to have arisen independently in these lineages since the paranasal sinuses, including the MS, were lost once in a common ancestor of extant OWMs (Rae et al., 2002). The performance of air conditioning depends mainly on how the air flows through the nasal cavity (Lindemann et al., 2004; Naftali et al., 2005; Kumahata et al., 2010; Hanida et al., 2013). The structures in the nasal cavity, especially in its anterior region, have major effects on the air-conditioning performance in humans (Lindemann et al., 2004; Naftali et al., 2005; Kumahata et al., 2010; Hanida et al., 2013). Nevertheless, in macaques, the MS topological differences suggests its functional role of air-conditioning performance (Marquez and Laitman, 2008) and the airflow in and out of the MS could affect the airflow within the nasal cavity that has some topological differences from that in humans.

In this study, we evaluated the air-conditioning performance using computational fluid dynamics (CFD) simulations based on a three-dimensional topological model of the nasal cavity and MS derived from the computed tomography (CT) scans of six macaques (including four *M. fuscata* and two *M. mulatta*) and a savanna monkey (*Chlorocebus aethiops*) (Fig. 1; Table S1). To evaluate the potential contributions of the MS to nasal passage airflow in macaques, we also generated nasal topology models where the MS was virtually removed for each subject of macaques, i.e., no-MS model.

We hypothesized that possible improvements in the air-conditioning performance and the contributions of the reacquired MS in macaques may have facilitated their successful adaptive radiation into various habitats.

RESULTS

We show the illustrations of visualizations in airflow and distributions of temperature and humidity for one subject representing all subjects among macaques (Figs 2, 3, 4), because all subjects here show comparable airflow pattern and air-conditioning performance. The illustrations in the other subjects are provided in Supporting Information (Figs S1, S2, S3).

The inhaled air flows almost horizontally and straight from the external nostril through the pharyngeal region, and the flow usually has a greater velocity through the middle regions compared with the peripheral regions of the nasal meatuses in macaques (Figs. 2A, D, S1). The CFD simulations using the no-MS model demonstrated that the airflow was almost the same as that in the normal model for each macaque (Figs. 2B, E, S1). Furthermore, similar airflow patterns were also found in a savanna monkey, which lacks the MS (Fig. 2F), and there were no noticeable distinctions between the two genera.

The size of the MS is restricted in Japanese macaques (average of 346 mm^3) compared with Rhesus macaques (average of 1254mm^3; Fig. 1). There is one ostium for each MS in all the subjects used here, while the ostium is varied in shape from almost circle to ellipse horizontally long. Regardless of this difference in MS anatomy, the inhaled air usually enters the MS from the posterior side of the ostium, which produces slow vortices within the MS, and it then exits the MS via the anterior side (Figs. 2C, S1). The flow within the MS reached up to 0.0005 m/s, which was far slower (>2,000 times) than that in the nasal cavity at the level of the ostium (average of 1.02 m/s) in both species of macaques.

In macaques and a savanna monkey, the temperature of the inhaled air was adjusted almost fully to 38.5°C, which is the temperature of the nasal organ set here, in the nasopharyngeal region with all three ambient atmospheric conditions (Table 1; Figs. 3A, C, S2). We found that the air was conditioned rapidly in the anterior region of the nasal cavity in these species (Figs. 3A, C, S2). The air was adjusted almost fully to 38.5°C at

the level of the ostium of the MS in both species of macaques, and the adjusted air then entered the MS (Figs. 3A, S2). This adjustment in temperature was also obtained in the no-MS models of macaques (Table 1; Figs. 3B, S2), and there were few differences in the temperature distributions of the normal and no-MS models; i.e., only up to 0.5°C in the mean value for the same frontal contour (Table 1; Figs. 3A, B, S2).

The mass fraction of water was also adjusted rapidly toward saturation at a given temperature, and it was fully saturated at 4.29% MF when the temperature was adjusted at 38.5°C—i.e., at 100% RH—in the anterior portion of the nasal cavity, which was the case in all atmospheric conditions for macaques and savanna monkeys (Table 1; Figs. 4A, C, S3). Thus, fully saturated air reached the ostium of the MS in macaques (Figs. 4A, S3). The same saturation performance was also obtained in the no-MS models of macaques (Table 1; Fig. 4B, S3), and there were few differences between the normal and no-MS models; i.e., up to 0.08% MF in the mean value for the same frontal contour (Table 1; Figs. 4A, B, S3).

DISCUSSION

Our CFD simulations demonstrated that the MS has few positive or negative effects on the airflow for air-conditioning within the nasal cavity of macaques. These minor contributions are probably attributable to the small ostium and the thin and long channel between the nasal cavity and the hollow of the MS (Fig. 1), and not to the volume of the MS. The airflow from the MS is too highly restricted and slow to modify the airflow within the nasal cavity in macaques, as seen in humans (Xiong et al., 2008; Na et al., 2012; Zhu et al., 2012). Thus, our bioengineered approach suggests that the reacquisition of the MS and its later anatomical modifications are functionally unrelated to the performance of air conditioning and the dispersal of macaques into cooler and dryer environments.

Many hypotheses have been proposed based on comparative morphology approaches to explain the physiological or mechanical functions related to the paranasal sinus including MS; e.g., cooling and regulation of the brain or orbital temperature, reactive reduction of the masticatory load on the cranium, acoustic modifications of nasalized voices, and air conditioning (Shea, 1977; Rae et al., 2003; Rae and Koppe, 2008; Curtis and Van Valkenburgh, 2014; Van Valkenburgh et al., 2014). The paranasal sinus is

often thought to reduce the weight of the cranium and save the bony materials by eliminating unnecessary bony resources (Rae and Koppe, 2004; Smith et al., 2005; Zollikofer and Weissmann, 2008). Although its biological advantages are still argued, this feature is believed to develop opportunistically from the middle meatus if there are few structural disturbances in that the pneumatization begins and progresses (Zollikofer and Weissmann, 2008; Smith et al., 2010). The paranasal sinus might develop and form as a spandrel, i.e., a feature passively formed by functional surrounding structures, but its evolutionary retention and inheritance in a given lineage should confer some evolutionary advantages that conquer some known disadvantages this feature has; e.g., risk of sinus inflammation, polypoids, and aplasia and hypoplasia, which produce malformation in the cheek surface and orbital floor (Dumonceaux et al., 1997; Koppe et al., 2006; Zimmermann et al., 2011; Nishimura and Ito, 2014). The advantages of such a spandrel-like feature are probably varied for different clades. The paranasal sinus is absent from most clades of the OWMs, but the MS re-emerged in the crown lineage of macaques since its ancestral loss from OWMs (Koppe and Ohkawa, 1999; Rae et al., 2002; Nishimura et al., 2014). Thus, the MS might confer specific functional advantages in macaques differently from the other primates and mammals. Future analyses of function, like the present approach, are expected to explain any adaptive significances of this feature for the crown group of macaques.

Furthermore, our study supports a scenario where macaques probably inherited a primitive faculty with excellent air conditioning, which facilitated their successful radiation into the temperate zone. The nasal cavity anatomy is often regarded as being evolutionarily sensitive to the ambient atmospheric conditions of a habitat in a given clade (Franciscus and Long, 1991; Rae et al., 2003; Marquez and Laitman, 2008), and thus the nasal region is often regarded as an independent functional module of the skull bony morphology; i.e., this region can be modified independently of the surrounding bony regions while maintaining their appropriate physiological functions (Anton, 1989). Nevertheless, the inhaled air is fully conditioned in the anterior portion of the nasal cavity in both macaques and savanna monkeys. These findings suggest that evolutionary modifications in the nasal anatomy, even in the anterior portion, can also be explained in terms of physiological or structural functions, as well as of air conditioning, at least in OWMs. This view is also supported by recent morphological

findings, which show that modifications of the nasal cavity are integrated with those in the neighboring cranial functional modules in humans and macaques, including the dentition, orbits and facial surfaces (Bastir and Rosas, 2013; Ito et al., 2015). Thus, the morphological variation in the nasal region might be only a weak response to the air-conditioning function in OWMs including macaques.

MATERIALS AND METHODS

Subjects and CT scanning

Six macaques—i.e., four Japanese macaques (*Macaca fuscata*, female) and two Rhesus macaques (*M. mulatta*, one male and one female)—and one savanna monkey (*Chlorocebus aethiops*, male), which were reared at the Primate Research Institute, Kyoto University (KUPRI), Inuyama, Japan, were scanned using a CT scanner (Asteion Premium 4, Toshiba Medical Systems Co.) at the same institute (Fig. 1; Table S1). Rhesus macaques are distributed in tropical and subtropical areas from western to eastern Asia. The savanna monkey is an OWM that lacks a MS, and it is distributed in tropical Africa. All of the subjects were anesthetized intramuscularly with 2.5 mg ketamine hydrochloride (Ketalar®, Daiichi Sankyo Propharma, Tokyo, Japan) and 0.1 mg medetomidine hydrochloride (Domitor®, Nippon Zenyaku Kogyo Co., Ltd., Fukushima, Japan) per kilogram of body weight before CT scanning. All of the experiments were performed in accordance with the third edition of the Guidelines for the Care and Use of Laboratory Primates at KUPRI, and the experimental protocol was approved by the Animal Welfare and Care Committee of the same institute.

All of the CT scans obtained in this study came from subjects without any history of surgery and had few abnormal traits in their heads, and few artifacts distorted the images of the nasal region. The scans were registered under PRICT # (Table S1) and are available via the website of the Digital Morphology Museum of KUPRI (dmm.pri.kyoto-u.ac.jp/archive/index.html).

Reconstruction of nasal topology models

Voxel data for the nasal cavity and MS anatomy were reconstructed from the CT scans (Kumahata et al., 2010; Hanida et al., 2013). The black areas represented air filling the nasal cavity, and the MS was extracted first using Avizo 7 (FEI Visualization

Sciences Group, Hiilsboro, OH, USA) based on a threshold of brightness, and the voxel data were reconstructed. After converting the voxel data into STereoLithography (STL) data, they were modified into data that represented a smooth surface using Magics 9.5 (Materialize Inc., Leuven, Belgium). Finally, a tetrahedron mesh with the mesh size of $\Delta x=3.0\times10^{-3}$ mm was generated from the modified STL data using Gambit 2.4 (ANSYS Inc., Canonsburg, PA, USA). The computational meshes had 1 to 3 million tetrahedral cells. The present solutions are evaluated independently to the mesh size: there were few differences between the solutions by the mesh size of $\Delta x= 0.18$ to 0.40×10^{-3} mm (the minimum size depends on the STL data size in each subject); i.e., up to 0.10% MF and 1.0°C in the mean value for the same frontal contour at the anterior nasal region, and up to 0.01% MF and 0.0°C at the posterior nasal and nasopharyngeal regions.

To evaluate the potential contributions of the MS to nasal passage airflow in macaques, we also generated no-MS model from the original tetrahedron mesh data for each subject.

Calculation methods

We performed steady-state analyses to examine the airflow, where the turbulence model was not employed. A steady simulation is reasonable under a normal breathing frequency and flow rate in the resting stage in humans (Swift and Proctor, 1977; Hornung et al., 1987; Hahn et al., 1993; Schreck et al., 1993; Keyhani et al., 1995; Doorly et al., 2008; Kumahata et al., 2010; Hanida et al., 2013). The maximum Reynolds numbers ranges from 85 to 555 at the external nostrils in the subjects use here, by calculated with estimates of the inhaled air velocity in the resting stage. They are lower than the critical Reynolds number (Swift and Proctor, 1977; Delson, 1980; Elad et al., 2008). The nasal flow is regarded as being mostly laminar in the resting stage of the subject used here. The Strouhal number value for the system is less than 0.25 (Doorly et al., 2008). Moreover, the Womersley number for human breathing is small, thereby indicating that any inertial effects on the flow pattern may be regarded as negligible (Doorly et al., 2008; Spence et al., 2012). We used the CFD simulation model developed by Hanida et al. (2013) to model an incompressible, viscid, laminar airflow in the nasal cavity with heat and water transport. The equations were solved using the fluid simulation software FLUENT 6.3 (ANSYS, Inc.).

The simulations were governed by the Navier–Stokes equation—i.e., the conservation of momentum equation (Eqn 1)—by the conservation of mass equation (Eqn 2), by the transport of energy equation (Eqn 3) and by the transport of the mass fraction of water equation (Eqn 4):

$$\rho\left\{\frac{\partial u}{\partial t}+(u\cdot\nabla)u\right\}=-\nabla p+\mu\nabla^2 u \tag{1}$$

$$\nabla\cdot u=0 \tag{2}$$

$$\rho Cp\left\{\frac{\partial T}{\partial t}+(u\cdot\nabla)T\right\}=K\nabla^2 T \tag{3}$$

$$\frac{\partial F}{\partial t}+(u\cdot\nabla)F=D\nabla^2 F \tag{4}$$

where t, u, p, ρ, μ, K, T, Cp, F and D denote time, velocity, pressure, density, kinematic viscosity, thermal conductivity, temperature, specific heat, the mass fraction of water and the mass diffusion coefficient, respectively. We regarded a solution as being of steady-state, after time advanced, i.e., we repeated the steps of calculation sufficiently.

Wall model for heat and water exchange

Heat and water are exchanged via the wall of the nasal cavity and the MS (if present). The wall comprises a vascular layer and mucous membrane. The wall was modeled as the organ and membrane layers (Fig. S4) to simulate the exchange of heat and water from the vascular layer to the air via mucous membrane (Hanida et al., 2013). The mucous membrane includes membrane epithelia, nasal glands, blood vessels and capillary blood vessels (Lang, 1989), and thus it varies in thickness between 0.3 mm and 5 mm, according to its location. The model comprised a smooth surface with a constant thickness of 0.5 mm, which was specified to simulate the actual performance in humans, after Hanida et al. (2013). Thus, the predicted air-conditioning performance may be slightly worse than that actually found in small-bodied monkeys having the thinner mucous membrane making the heat and water exchange efficient compared to thick one in humans. The optimum solution values for the temperature and humidity of the air were calculated by setting a boundary condition that represented heat and water exchange via the surface of the membrane layer.

Simulation model of heat and water exchange

Heat is transferred between the air and the organ layer via the membrane layer (Fig. S4A). The heat transport of Q_{memb} from the organ side is determined by Eqn 5. The latent heat of Q_{latent} is calculated from Eqn 6, where L and W_{bl} denote the specific latent heat and water flux from the surface of the membrane layer, respectively. L is defined by Eqn 7, which was calculated by cubic fitting to the data reported by (Rogers and Yau, 1989). The total heat transport, Q_{total}, is defined by Eqn 8 as a flux boundary condition for the energy equation (Eqn 3).

$$Q_{memb} = K_{memb} \frac{T_S - T_O}{\delta_{memb}} \tag{5}$$

$$Q_{latent} = -LW_{bl} \tag{6}$$

$$L = 2500.79 - 0.00000614342 \times T_S^3 + 0.00158927 \times T_S^2 - 2.36418 \times T_S \tag{7}$$

$$Q_{total} = Q_{memb} + Q_{latent} = K_{memb} \frac{T_S - T_O}{\delta_{memb}} - LW_{bl} \tag{8}$$

T_S, T_O, K_{memb} and δ_{memb} denote the temperature of the surface, the organ layer temperature, the thermal conductivity of the membrane layer and the membrane layer thickness, respectively. T_O is constant, and we set it to 38.5°C, which is the average body temperature measured in macaques. The thermal conductivity of the mucous membrane K_{memb} is 0.6 W/mK that is thermal conductivity of water (Lervik et al., 2010), because the liquid mucous membrane is assumed in the model used here (Kumahata et al., 2010; Hanida et al., 2013). T_S is determined by Q_{total}, which comprises Q_{memb} and Q_{latent}.

To simulate water exchange, the wall model was implemented with a boundary layer to define the boundary condition of species transport based on the Fick's law (Fig. S4B). According to the Fick's law, the flux diffusion is proportional to the concentration gradient of water. We used the Dirichlet-type boundary condition—i.e., fixed transport—in the FLUENT software. The two-film theory was used to evaluate the mass of species transport between a liquid phase and a gas phase across a boundary.

The thickness of the boundary layer was set to 0.5 mm (Hanida et al., 2013). W_{bl} is the water flux from the boundary layer, which is determined from Eqn 9, and this was used to calculate the latent heat of Eqns 6 and (8). W_{memb} is the water flux from the organ layer, which is determined from Eqn 10.

$$W_{bl} = D_{bl}\frac{F - F_S}{\delta_{bl}} \tag{9}$$

$$W_{memb} = D_{memb}\frac{F_S - F_O}{\delta_{memb}} \tag{10}$$

F, F_S, F_O, δ_{bl}, δ_{memb}, D_{bl} and D_{memb} denote the water fraction in the boundary layer, the water fraction on the membrane surface, the water fraction on the organ layer, the boundary layer thickness, the membrane layer thickness, the mass diffusion coefficient of the boundary layer and the mass diffusion coefficient of the membrane layer, respectively. D_{bl} and D_{memb} are 3.0×10^{-5} m^2/s and 2.6×10^{-5} m^2/s, respectively (Lee and Wilke, 1954). F_O is 4.29% of the mass fraction of water (% MF) with 100% relative humidity (% RH) at 38.5°C. It should be noted that diffusion in the boundary layer is greater than that in the membrane layer (Kumahata et al., 2010; Hanida et al., 2013). The water flux is transported from the organ through the membrane and boundary layers to the air. Simultaneously solving Eqns 9 and 10 for F_S gives Eqn 11. The temperature is not dominant in Eqns 9–11, and the water transport is not regarded as being dependent on a temperature in this model. To enable the mass flux of species transport, F_S was fixed as the boundary condition for water exchange. This boundary condition was implemented as a user-defined function in FLUENT software.

$$F_S = \frac{\left(\frac{D_{memb}}{\delta_{memb}}\right)F_O - \left(\frac{D_{bl}}{\delta_{bl}}\right)F}{\left(\frac{D_{memb}}{\delta_{memb}}\right) + \left(\frac{D_{bl}}{\delta_{bl}}\right)} \tag{11}$$

Calculation conditions

The external nostril was modeled as a free inlet, and no-slip boundary conditions were applied at the walls, while the outward velocity was assigned at the pharynx.

The time-average speed of inhaled air was calculated based on estimates of the resting tidal volume and the respiratory rate, as well as the measurement of the

cross-sectional area of the pharyngeal region at a given position for each subject (Table S1). The cross-sectional area was calculated at a given location in the pharynx based on the CT scans using Magics software.

The resting tidal volume was estimated using Eqn 12 (Worthington et al., 1991):

$$TV = 7.69\,BW^{1.04} \tag{12}$$

TV and BW are the estimates of the resting tidal volume (ml) and the measured body weight (kg), respectively.

The resting respiratory rate was estimated using Eqn 13 (Stahl, 1967):

$$f = 0.84\,BW^{-0.26} \tag{13}$$

f denotes the estimated respiratory rate (times/second).

Finally, the time-averaged speed was calculated using Eqn 14:

$$FV = \frac{2f \times TV}{CA} \tag{14}$$

FV and CA denote the time-averaged flow velocity (m/s) and the measured cross-sectional area at a given location in the pharyngeal region (mm^2), respectively.

The CFD simulations were performed in three ambient atmospheric air conditions: cold–dry, 10% RH at 5°C (0.05% MF); hot–dry, 5% RH at 40°C (0.23% MF); and warm–wet, 90% RH at 30°C (2.38% MF).

Visualizations

The resulting spatial pattern of the vector quantity representing the velocity and direction of the airflow is illustrated using streamlines in different colors that was computed from the points on the plane of external nostrils (Kumahata et al., 2010; Hanida et al., 2013). Those of the scalar quantity representing the temperature and water vapor volume are illustrated using contours in different colors (Kumahata et al., 2010; Hanida et al., 2013).

Acknowledgements

The authors thank A. Kaneko, S. Funahashi, H. Koda, T. Kunieda, and A. Kato for help with CT scanning.

Competing interests

No competing interest declared

Author contributions

T.N. and F.M. designed research, T.N., T.M.-N., J.S. scanned macaques, F.M., S.H., K.K., and T. M. carried out the CFD simulations, T.N., F.M., S.H., and T.M. discussed the results, T.N. and F.M. wrote the paper.

Funding

This work was supported financially by the Asahi Grass Foundation, Tokyo, Japan [to T.N.], by the Japan Society for the Promotion of Science [Grants-in-Aid for Scientific Research, 26650171 to T.D.N. Nishimura and 26304019 to M.Takai, Strategic Young Researcher Overseas Visits Program for Accelerating Brain Circulation, to T.D.N.].

Supplementary material

Supplementary material available online at

References

Alba, D. M., Delson, E., Carnevale, G., Colombero, S., Delfino, M., Giuntelli, P., Pavia, M. and Pavia, G. (2014). First joint record of *Mesopithecus* and cf. *Macaca* in the Miocene of Europe. *J. Hum. Evol.* **67**, 1–18.

Anton, S. C. (1989). Intentional cranial vault deformation and induced changes of the cranial base and face. *Am. J. Phys. Anthropol.* **79**, 253–267.

Bastir, M. and Rosas, A. (2013). Cranial airways and the integration between the inner and outer facial skeleton in humans. *Am. J. Phys. Anthropol.* **152**, 287–293.

Cave, A. J. E. (1973). The primate nasal fossa. *Proc. Linn. Soc. London* **5**, 377–387.

Cole, P. (1982). Modification of inspired air. In *The Nose: Upper Airway Physiology and the Atmospheric Environment* (ed. D. F. A. Proctor and I. Anderseb), pp. 350–375. Amsterdam: Elsevier Biomedical Press.

Curtis, A. A. and Van Valkenburgh, B. (2014). Beyond the sniffer: frontal sinuses in Carnivora. *Anat. Rec.* **297**, 2047–2064.

Delson, E. (1980). Fossil macaques, phyletic relationships and a scenario of deployment. In *The Macaques: Studies in Ecology, Behavior, and Evolution* (ed. D. G. Lindburg), pp. 10–30. New York: Van Nostrand Reinhold.

Doorly, D. J., Taylor, D. J. and Schroter, R. C. (2008). Mechanics of airflow in the human nasal airways. *Respir. Physiol. Neurobiol.* **163**, 100–110.

Dumonceaux, G. A., Lamberski, N., Clutter, D., Nagy, S. M., Jr., Burek, K. and Phillips, L. G. (1997). Treatment of bilateral nasal polyposis and chronic refractory inhalant allergic rhinitis in a chimpanzee (*Pan troglodytes*). *J. Zoo Wildl. Med.* **28**, 215–219.

Elad, D., Wolf, M. and Keck, T. (2008). Air-conditioning in the human nasal cavity. *Respir. Physiol. Neurobiol.* **163**, 121–127.

Fleagle, J. G. (2013). Primate Adaptation and Evolution. Amsterdam: Academic Press.

Fooden, J. (1980). Classification and distribution of living macaques (*Macaca* Lacepede, 1799). In *The Macaques: Studies in Ecology, Behavior, and Evolution* (ed. D. G. Lindburg), pp. 1–9. New York: Van Nostrand Reinhold.

Fooden, J. and Albrecht, G. H. (1993). Latitudinal and insular variation of skull size in crab-eating macaques (Primates, Cercopithecidae: *Macaca fascicularis*). *Am. J. Phys. Anthropol.* **92**, 521–538.

Franciscus, R. G. and Long, J. C. (1991). Variation in human nasal height and breadth. *Am. J. Phys. Anthropol.* **85**, 419–427.

Hahn, I., Scherer, P. W. and Mozell, M. M. (1993). Velocity profiles measured for airflow through a large-scale model of the human nasal cavity. *J. Appl. Physiol. (1985)* **75**, 2273–2287.

Hanida, S., Mori, F., Kumahata, K., Watanabe, M., Ishikawa, S. and Matsuzawa, T. (2013). Influence of latent heat in the nasal cavity. *J. Biomech. Sci. Eng.* **8**, 209–224.

Harkema, J. R., Plopper, C. G., Hyde, D. M., Wilson, D. W., St George, J. A. and Wong, V. J. (1987). Nonolfactory surface epithelium of the nasal cavity of the bonnet monkey: a morphologic and morphometric study of the transitional and respiratory epithelium. *Am. J. Anat.* **180**, 266-279.

Hornung, D. E., Leopold, D. A., Youngentob, S. L., Sheehe, P. R., Gagne, G. M., Thomas, F. D. and Mozell, M. M. (1987). Airflow patterns in a human nasal model. *Arch. Otolaryngol. Head Neck Surg.* **113**, 169–172.

Ito, T., Nishimura, T. and Takai, M. (2014). Ecogeographical and phylogenetic effects on craniofacial variation in macaques. *Am. J. Phys. Anthropol.* **154**, 27–1.

Ito, T., Nishimura, T. D., Hamada, Y. and Takai, M. (2014). Contribution of the maxillary sinus to the modularity and variability of nasal cavity shape in Japanese macaques. *Primates* **in press**.

Keyhani, K., Scherer, P. W. and Mozell, M. M. (1995). Numerical simulation of airflow in the human nasal cavity. *J. Biomech. Eng.* **117**, 429–441.

Koppe, T. and Ohkawa, Y. (1999). Pneumatization of the facial skeleton in catarrhine primates. In *The Paranasal Sinuses of Higher Primates:*

Development, Function, and Evolution (ed. T. Koppe, H. Nagai and K. W. Alt), pp. 77–119. Berlin: Quintessence.

Koppe, T., Rohrer-Ertl, O., Breier, S. and Wallner, C. P. (2006). Maxillary sinus atelectasis in a wild born gibbon (*Hylobates moloch*). *Primates* **47**, 140–144.

Kumahata, K., Mori, F., Ishikawa, S. and Matsuzawa, T. (2010). Nasal flow simulation using heat and humidity models. *J. Biomech. Sci. Eng.* **5**, 565–577.

Lang, J. (1989). Clinical Anatomy of the Nose, Nasal Cavity, and Paranasal Sinuses. New York: George Thieme Verlag.

Lee, C. Y. and Wilke, C. R. (1954). Measurements of vapor diffusion coefficient. *Ind. Eng. Chem.* **46**, 2381–2387.

Lervik, A., Bresme, F., Kjelstrup, S., Bedeaux, D. and Miguel Rubi, J. (2010). Heat transfer in protein-water interfaces. *Phys. Chem. Chem. Phys.* **12**, 1610–1617.

Lindemann, J., Keck, T., Wiesmiller, K., Sander, B., Brambs, H. J., Rettinger, G. and Pless, D. (2004). A numerical simulation of intranasal air temperature during inspiration. *Laryngoscope* **114**, 1037–1041.

Marquez, S. and Laitman, J. T. (2008). Climatic effects on the nasal complex: a CT imaging, comparative anatomical, and morphometric investigation of *Macaca mulatta* and *Macaca fascicularis*. *Anat. Rec.* **291**, 1420–1445.

Na, Y., Kim, K., Kim, S. K. and Chung, S. K. (2012). The quantitative effect of an accessory ostium on ventilation of the maxillary sinus. *Respir. Physiol. Neurobiol.* **181**, 62–73.

Naftali, S., Rosenfeld, M., Wolf, M. and Elad, D. (2005). The air-conditioning capacity of the human nose. *Ann. Biomed. Eng.* **33**, 545–553.

Nishimura, T., Ito, T., Yano, W., Ebbestad, J. O. R. and Takai, M. (2014). Nasal architecture in *Procynocephalus wimani* (Early Pleistocene, China) and implications for its phyletic relationship with Paradolichopithecus. *Anthropol. Sci.* **122**, 101–113.

Nishimura, T. D. and Ito, T. (2014). Aplasia of the maxillary sinus in a Tibetan macaque (*Macaca thibetana*) with implications for its evolutionary loss and reacquisition. *Primates* **55**, 501–508.

Pan, R.-L. and Oxnard, C. (2000). Craniodental variation of macaques (*Macaca*): size, function and phylogeny. *Zool. Res.* **21**, 308–322.

Rae, T. C. and Koppe, T. (2004). Holes in the head: evolutionary interpretations of the paranasal sinuses in catarrhines. *Evol. Anthropol.* **13**, 211–223.

Rae, T. C. and Koppe, T. (2008). Independence of biomechanical forces and craniofacial pneumatization in *Cebus*. *Anat. Rec.* **291**, 1414–1419.

Rae, T. C., Hill, R. A., Hamada, Y. and Koppe, T. (2003). Clinal variation of maxillary sinus volume in Japanese macaques (*Macaca fuscata*). *Am. J. Primatol.* **59**, 153–158.

Rae, T. C., Koppe, T., Spoor, F., Benefit, B. and McCrossin, M. (2002). Ancestral loss of the maxillary sinus in Old World monkeys and independent acquisition in *Macaca*. *Am. J. Phys. Anthropol.* **117**, 293–296.

Rogers, R. R. and Yau, M. K. (1989). A Short Course in Cloud Physics. Oxford: Pergamon Press.

Rossie, J. B. (2008). The phylogenetic significance of anthropoid paranasal sinuses. *Anat. Rec.* **291**, 1485–1498.

Schreck, S., Sullivan, K., Ho, C. and Chang, H. (1993). Correlations between flow resistance and geometry in a model of the human nose. *J. Appl. Physiol.* **75**, 1767–1775.

Shea, B. T. (1977). Eskimo craniofacial morphology, cold stress and the maxillary sinus. *Am. J. Phys. Anthropol.* **47**, 289–300.

Smith, T. D., Rossie, J. B., Cooper, G. M., Mooney, M. P. and Siegel, M. I. (2005). Secondary pneumatization of the maxillary sinus in callitrichid primates: insights from immunohistochemistry and bone cell distribution. *Anat. Rec.* **285**, 677–689.

Smith, T. D., Rossie, J. B., Cooper, G. M., Carmody, K. A., Schmieg, R. M., Bonar, C. J., Mooney, M. P. and Siegel, M. I. (2010). The maxillary sinus in three genera of New World monkeys: factors that constrain secondary pneumatization. *Anat. Rec.* **293**, 91–107.

Spence, C. J. T., Buchmann, N. A. and Jermy, M. C. (2012). Unsteady flow in the nasal cavity with high flow therapy measured by stereoscopic PIV. *Exp. Fluids* **52**, 569–579.

Stahl, W. R. (1967). Scaling of respiratory variables in mammals. *J. Appl. Physiol.* **22**, 453–460.

Swift, D. L. and Proctor, D. F. (1977). Access of air to the respiratory tract. In *Respiratory Defense Mechanisms*, vol. 5 (ed. J. D. Brain, D. F. Proctor and L. M. Reid), pp. 63–93. New York: Marcel Dekker.

van Valkenburgh, B., Smith, T. D. and Craven, B. A. (2014). Tour of a labyrinth: exploring the vertebrate nose. *Anat. Rec.* 297, 1975–1984.

Worthington, J., Young, I. S. and Altringham, J. D. (1991). The relationship between body-mass and ventilation rate in mammals. *J. Exp. Biol.* **161**, 533–536.

Xiong, G. X., Zhan, J. M., Jiang, H. Y., Li, J. F., Rong, L. W. and Xu, G. (2008). Computational fluid dynamics simulation of airflow in the normal nasal cavity and paranasal sinuses. *Am. J. Rhinol.* **22**, 477–482.

Zhu, J. H., Lee, H. P., Lim, K. M., Gordon, B. R. and Wang de, Y. (2012). Effect of accessory ostia on maxillary sinus ventilation: a computational fluid dynamics (CFD) study. *Respir. Physiol. Neurobiol.* **183**, 91–99.

Zimmermann, N., Pirovino, M., Zingg, R., Clauss, M., Kaup, F. J., Heistermann, M., Hatt, J. M. and Steinmetz, H. W. (2011). Upper respiratory tract disease in captive orangutans (*Pongo* sp.): prevalence in 20 European zoos and predisposing factors. *J. Med. Primatol.* **40**, 365–375.

Zollikofer, C. P. E. and Weissmann, J. D. (2008). A morphogenetic model of cranial pneumatization based on the invasive tissue hypothesis. *Anat. Rec.* **291**, 1446–1454.

Figures

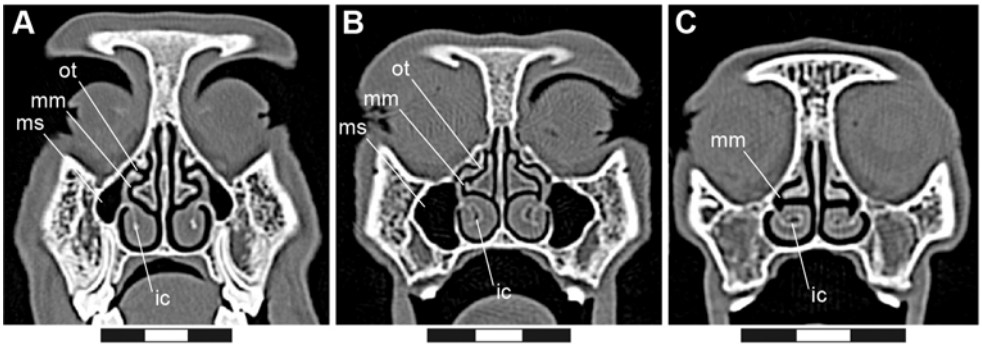

Fig. 1. Frontal CT scans. (A) Japanese macaque, *Macaca fuscata*, Mff765 (CT scan id, PRICT-369); (B) Rhesus monkey, *M. mulatta*, Mm1701 (PRICT-394); and (C) savanna monkey, *Chlorocebus aethiops*, Ca14 (PRICT-27). Abbreviations: ic, inferior concha; mm, middle meatus; ms, maxillary sinus; ot, ostium. The scale is in centimeters.

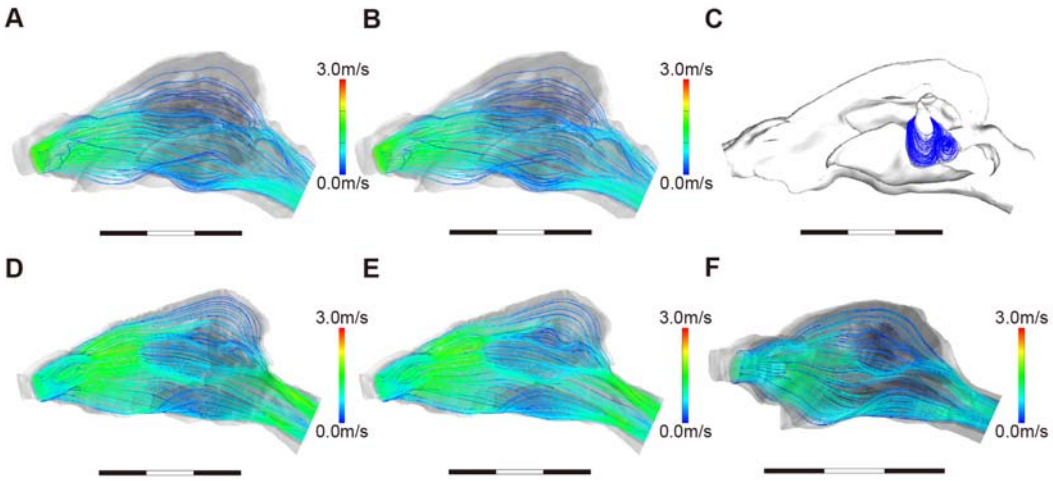

Fig. 2. Airflows and flow velocity in the nasal cavity and within the maxillary sinus. The airflow in the nasal cavity simulated with (A) the normal model and (B) the no-MS model, and (C) the airflow within the maxillary sinus, for a Japanese macaque, *Macaca fuscata*, Mff765 (PRICT-369), female. The airflow in the nasal cavity simulated with (D) the normal model and (E) the no-MS model for rhesus macaque, *M. mulatta*, Mm1715m (PRICT-395), male. (F) The airflow for a savanna monkey, *Chlorocebus aethiops*, Ca14 (PRICT-27), male. The streamline indicates the airflow direction and velocity distributions throughout the nasal passage. The streamline number reflects the airflow volume. The scale is in centimeters.

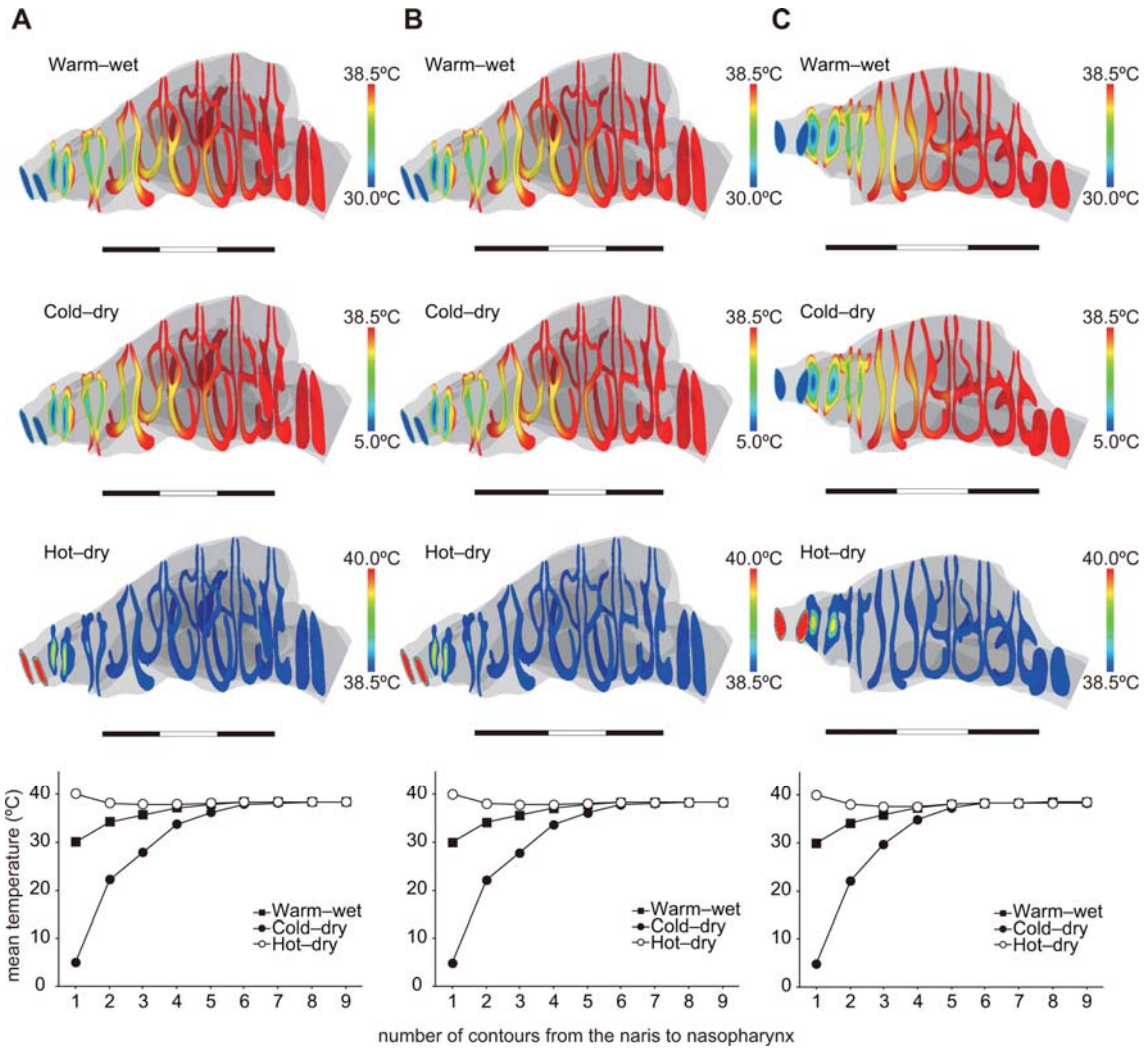

Fig. 3. Temperature distributions in the nasal passage. The contours represent the temperature distributions at each level from the nares to the nasopharynx, which were simulated with (A) the normal model and (B) the no-MS model for Japanese macaques, *Macaca fuscata*, Mff765 (PRICT-369), female; and (C) for a savanna monkey, *Chlorocebus aethiops*, Ca14 (PRICT-27), male. The mean temperature values for each contour from the nostril to nasopharynx (bottom) indicate the performance when adjusting the temperatures to 38.5°C. The scale is in centimeters.

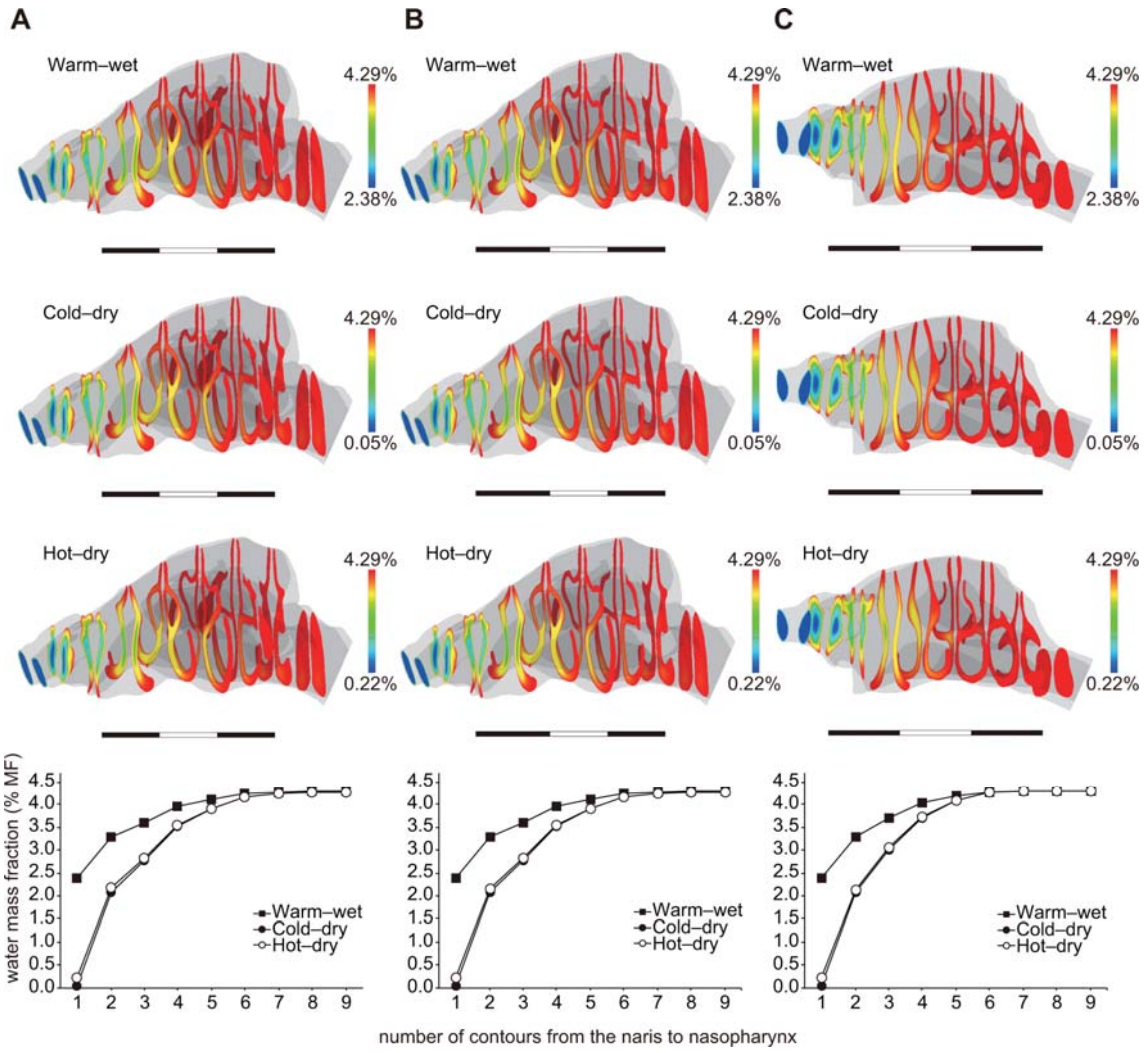

Fig. 4. Water mass distributions in the nasal passage. The contours represent the distributions of the water mass fraction at each level from the nares to the nasopharynx, which were simulated with (A) the normal model and (B) the no-MS model for Japanese macaques, *Macaca fuscata*, Mff765 (PRICT-369), female; (C) and for a savanna monkey, *Chlorocebus aethiops*, Ca14 (PRICT-27), male. The mean water mass values for each contour from the nostril to nasopharynx (bottom) indicate the performance of water vapor transport in the inhaled air to 4.29% MF. The scale is in centimeters.

Table 1. Mean values of temperature and water mass fraction at the nasopharyngeal level.

Subjects		Warm and wet		Cold and dry		Hot and dry	
		Temp. (℃)	MF (%)	Temp. (℃)	MF (%)	Temp. (℃)	MF (%)
Japanese macaques, *Macaca fuscata*							
Mff765	MS	38.5	4.28	38.4	4.27	38.5	4.27
	no-MS	38.5	4.28	38.4	4.27	38.5	4.27
Mff963	MS	38.4	4.27	38.3	4.25	38.4	4.25
	no-MS	38.4	4.27	38.3	4.25	38.4	4.25
Mff1859	MS	38.5	4.29	38.5	4.29	38.5	4.29
	no-MS	38.5	4.30	38.5	4.30	38.5	4.30
Mff2115	MS	38.7	4.30	38.5	4.30	38.5	4.30
	no-MS	38.5	4.30	38.5	4.29	38.5	4.29
Rhesus macaques, *Macaca mulatta*							
Mm1701	MS	38.5	4.30	38.5	4.30	38.5	4.30
	no-MS	38.5	4.30	38.5	4.30	38.5	4.30
Mm1715	MS	38.5	4.30	38.5	4.30	38.5	4.30
	no-MS	38.5	4.29	38.5	4.29	38.5	4.29
Savanna monkeys, *Chlorocebus aethiops*							
Ca40		38.5	4.29	38.5	4.29	38.5	4.29

abbreviations: Temp, temperature; MF, water mass fraction; MS and no-MS, MS and no-MS model of the nasal cavity.

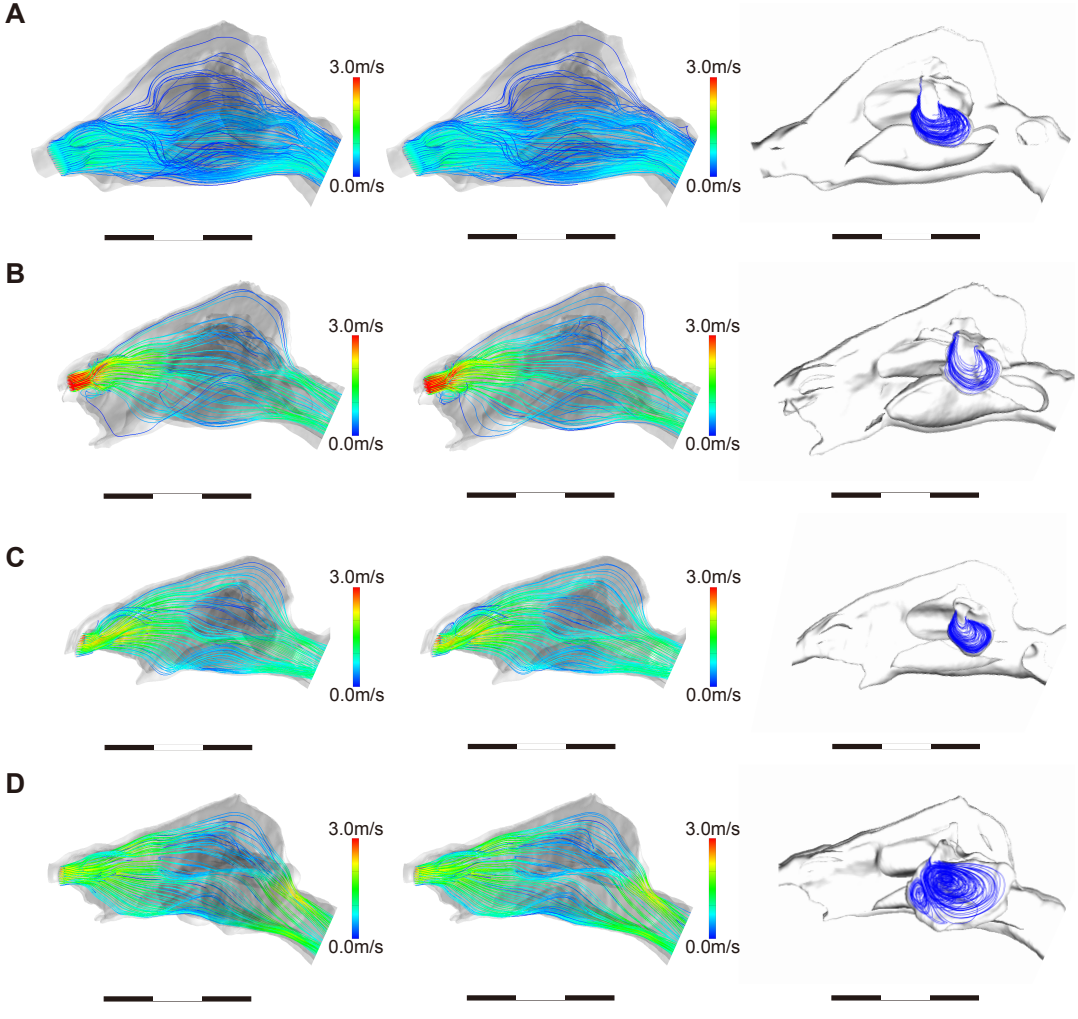

Fig. S1. Airflows and flow velocity in the nasal passage and within the maxillary sinus (MS). (A) Japanese macaque, *Macaca fuscata* (Mff963); (B) *M. fuscata* (Mff1859); (C) *M. fuscata* (Mff2115); (D) rhesus macaque, *M. mulatta* (Mm1701). The airflow was simulated using the normal model (left) and the no-MS model (middle). The streamline indicates the airflow direction, where the number and colour reflect the airflow volume and velocity, respectively. The vortex airflow within the MS (right) was far slower than that in the nasal cavity. The scale is in centimeters.

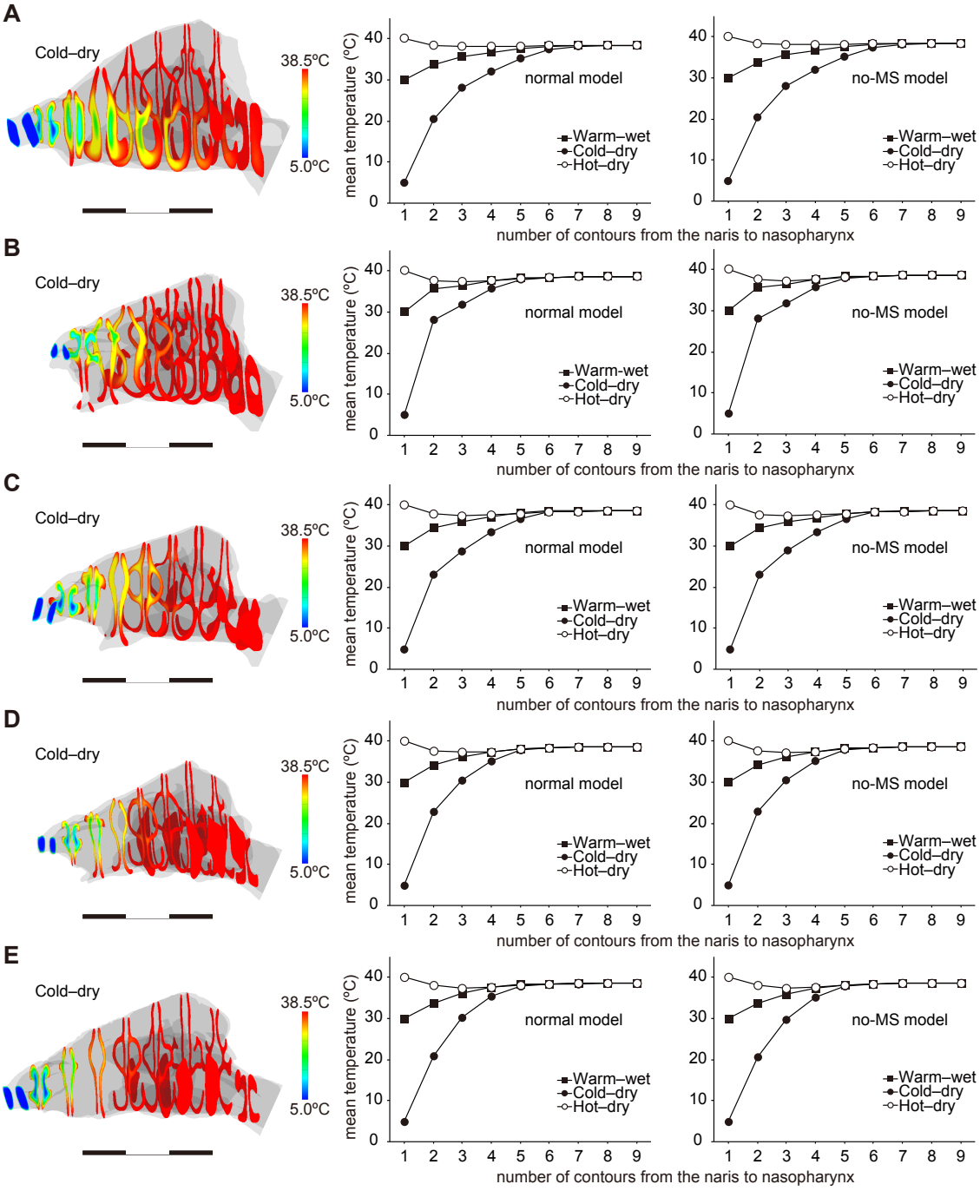

Fig. S2. Temperature distributions in the nasal passage. (A) Japanese macaque, *Macaca fuscata* (Mff963); (B) *M. fuscata* (Mff1859); (C) *M. fuscata* (Mff2115); (D) rhesus macaque, *M. mulatta* (Mm1701); and (E) *M. mulatta* (Mm1715). The mean temperature values for each contour, which were simulated with the normal model (middle) and the no-MS model (right), indicate the performance of adjusting the temperature to 38.5°C.

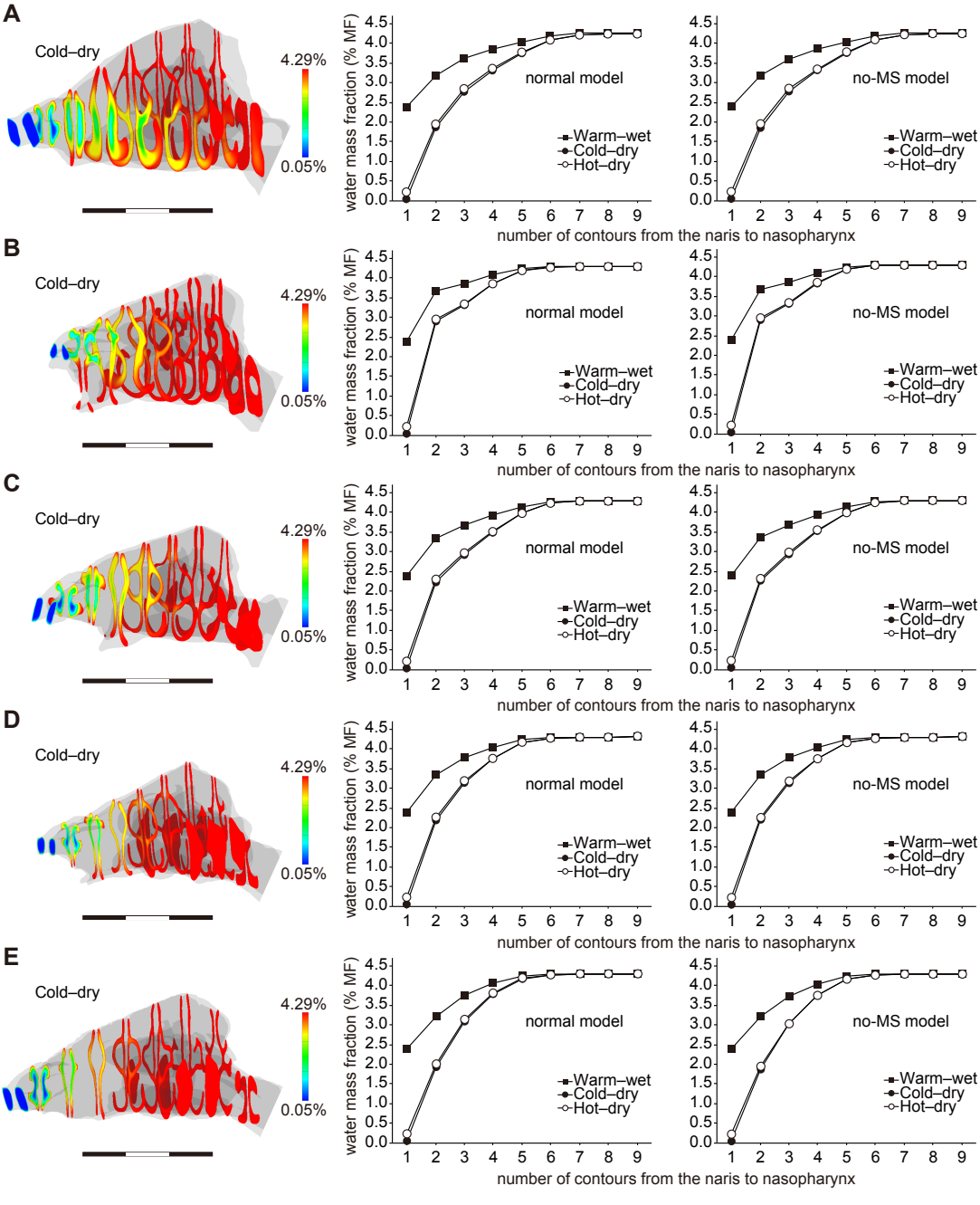

Fig. S3. Water mass distributions in the nasal passage. (A) Japanese macaque, *Macaca fuscata* (Mff963); (B) *M. fuscata* (Mff1859); (C) *M. fuscata* (Mff2115); (D) rhesus macaque, *M. mulatta* (Mm1701); and (E) *M. mulatta* (Mm1715). The mean water mass values for each contour from the nostril to nasopharynx, which were simulated with the normal model (middle) and the no-MS model (right), indicate the performance of water vapor transport in the inhaled air to 4.29% MF. The scale is in centimeters.

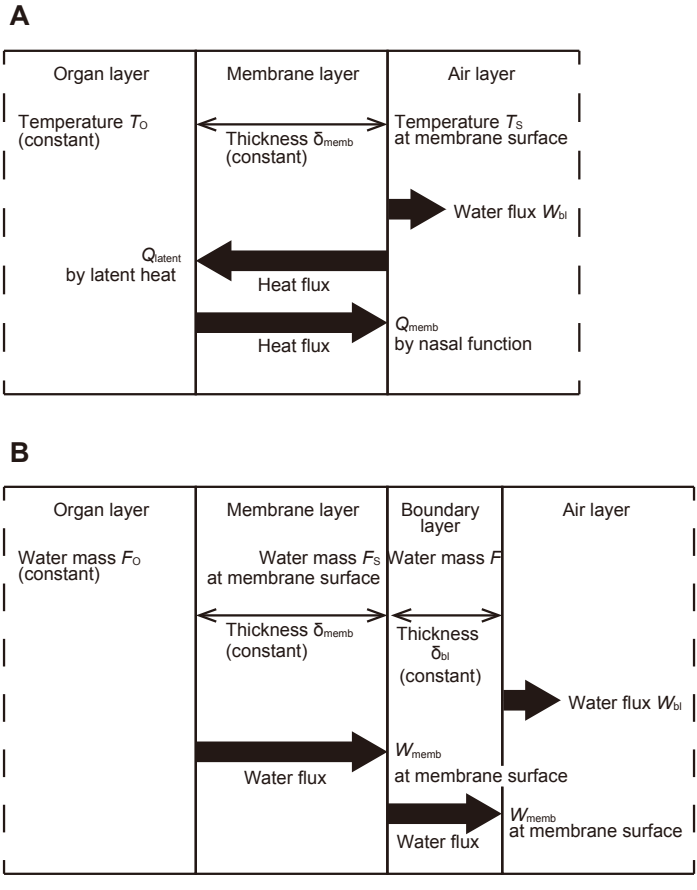

Fig. S4. Wall models of the nasal passage. (A) Model for heat exchange. Q_{memb}, Q_{latent} and W_{bl} indicate the heat flux of the nasal wall function, the heat flux of latent heat and the water flux from the boundary layers in (B), respectively. T_S, T_O and δ_{memb} are the temperature of the surface, the organ layer temperature and the membrane layer thickness, respectively. (B) Model for water exchange. W_{bl} and W_{memb} are the water flux from the boundary layer and the water flux from the organ layer, respectively. F, F_S, F_O and δ_{bl} are the water fraction in the boundary layer, the water fraction on the membrane surface, the water fraction on the organ layer and the boundary layer thickness, respectively.

Table S1. Subjects, scans and estimated respiration parameters.

				scans			respiration parameters			
subjects	sex	BW (kg)	age (yrs)	PRICT #*	resolution (mm/pixel)	interval (mm)	CA (mm^2)	TV (ml)	f (times/s)	FV (m/s)
Japanese macaque, *Macaca fuscata*										
Mff765	female	10.2	28	369	0.225	0.20	74	86.1	0.459	1.070
Mff963	female	6.6	26	374	0.250	0.20	258	54.7	0.514	0.218
Mff1859	female	8.7	9	46	0.263	0.20	122	73.0	0.479	0.572
Mff2115	female	7.9	5	380	0.125	0.20	210	66.0	0.491	0.308
Rhesus monkey, *Macaca mulatta*										
Mm1701	female	6.7	6	394	0.225	0.20	71	55.6	0.512	0.802
Mm1715	male	7.1	6	395	0.250	0.20	131	59.1	0.505	0.455
Savanna monkey, *Chlorocebus aethiops*										
Ca14	male	3.8	23	27	0.200	0.20	116	30.7	0.594	0.314

abbreviations: CA, cross-sectional area at the oropharyngeal level; TV, estimated tidal volume; f, estimated frequency of breath; FV, flow velocity at the pharyngeal level.

* The scans are registered on the website of the Digital Mo phology Museum (DMM) at KUPRI (http://dmm.pri.kyoto-u.ac.jp/archive/).

†estimated using the formula $TV = 7.69\,BW^{1.04}$

‡estimated using the formula $f = 0.84\,BW^{-0.26}$

§calculated using the formula $FV = \frac{2f \times TV}{CA}$